ACS APPLIED ENERGY MATERIALS

www.acsaem.org Article

Temperature-Dependent Electroabsorption Spectra and Exciton Binding Energy in a Perovskite $CH_3NH_3PbI_3$ Nanocrystalline Film

Morihiko Hamada,[§] Shailesh Rana,[§] Efat Jokar, Kamlesh Awasthi, Eric Wei-Guang Diau, and Nobuhiro Ohta*

Cite This: *ACS Appl. Energy Mater.* 2020, 3, 11830−11840 Read Online

ACCESS | Metrics & More | Article Recommendations | Supporting Information

ABSTRACT: Temperature-dependent electroabsorption (E-A) spectra of methylammonium lead tri-iodide ($MAPbI_3$) solid film, which result from the quadratic Stark effect of the exciton absorption band, have been analyzed with an integral method. The change in the electric dipole moment ($\Delta\mu$) and polarizability ($\Delta\alpha$) following exciton absorption was determined at each temperature; the absorption profile was separated into an exciton band and a continuum band caused by a transition from the valence band to the conduction band, and the position and the linewidth of the exciton absorption band were determined at each temperature. As the temperature decreased, a phase transition occurred from a tetragonal phase to an orthorhombic phase; the temperature dependence of $\Delta\mu$ and $\Delta\alpha$ differed greatly between the two phases. We have evaluated the exciton binding energy (E_B) of $MAPbI_3$ polycrystalline film with the following three methods: (1) fitting the temperature-dependent absorption profile; (2) fitting the temperature-dependent linewidth of the exciton absorption profile; and (3) fitting the photoluminescence intensity as a function of temperature. The E_B values thus determined for samples fabricated with the same procedure are compared. Our estimated binding energies for an exciton of a $MAPbI_3$ nanocrystalline film are also compared with those reported in the literature.

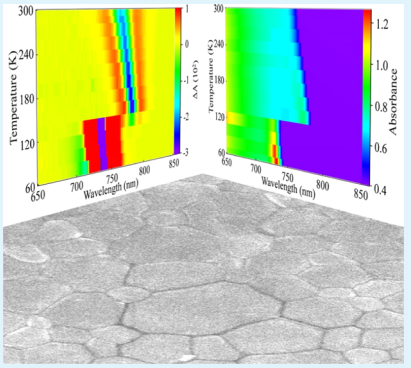

KEYWORDS: *temperature-dependent electroabsorption spectra, integral method analysis, methylammonium lead iodide perovskite, exciton binding energy, perovskite solar cells*

INTRODUCTION

Over the past few years, methylammonium lead halide ($MAPbX_3$) perovskites have become fascinating and purposeful materials for next-generation cheap optoelectronic devices, such as solar cells, field-effect transistors, light-emitting devices (LEDs), photodetectors, and memory devices.[1−7] The most satisfactory traits of these materials are that they are processable in solution and that they have unique optoelectronic properties, such as a tunable band gap, a wide emission region, long carrier diffusion lengths, and large carrier mobilities.[8−10] The performance of these perovskite materials varies with the fabrication. Methylammonium lead tri-iodide ($MAPbI_3$), which is the most studied perovskite, has attained the great efficiency of conversion of photons to electrical power, but the binding energy of an exciton produced on photoexcitation is still debated.[11]

To advance scientific techniques, the application of the electric field has been used to design and develop more efficient optoelectronic devices.[12−14] The performance of a perovskite-based optoelectronic device depends on an external electric field, indicating that the performance of a photovoltaic cell can be improved by applying an external electric field.[13,14] Application of an electric field can be used also to understand the working mechanism of an optoelectronic device. Many studies have been devoted to the effect of an electric field on the optical properties of lead halide perovskites.[15−24] Electric-field modulation spectra provide information to understand the excitonic feature in a semiconductor as an unwanted background signal becomes suppressed by means of an electric field.[25]

Ziffer et al. reported electroabsorption (E-A) spectra of $MAPbI_3$,[17] i.e., the effects of an electric field on absorption spectra; the E-A spectra observed at the second harmonic of the modulation frequency ($2f$) of an applied electric field were related to the Franz−Keldysh−Aspnen (FKA) effect, as observed in other bulk semiconductors whose binding energy of an exciton is less than 10 meV. As mentioned in our previous paper, the E-A spectra of $MAPbI_3$ observed at the second harmonic of the modulation frequency were interpreted in terms of the quadratic Stark effect of the exciton absorption band for these reasons: (1) the field-

Received: August 17, 2020
Accepted: November 13, 2020
Published: November 27, 2020

https://dx.doi.org/10.1021/acsaem.0c01983
ACS Appl. Energy Mater. 2020, 3, 11830−11840

induced change in absorption intensity is proportional to the square of the strength of the applied electric field; (2) the FKA oscillation, which is expected in the continuum band in the presence of an applied electric field,[26] was observed at neither room temperature nor low temperature, although the E-A spectra of $MAPbI_3$ at low temperatures were not shown explicitly; and (3) the third derivative of the absorption spectra, of which the E-A spectra have a shape expected according to the FKA model,[27] had a shape that differed greatly from the observed E-A spectra of a $MAPbBr_3$ nanocrystalline film, which shows the E-A spectra similar to that of $MAPbI_3$. In the results, the change in electric dipole moment and polarizability following photoexcitation into the exciton band is expected to be estimated through the analysis of the E-A spectra of $MAPbI_3$ at different temperatures.

Independently of our work on the E-A spectra of $MAPbI_3$,[20] the E-A spectra of $MAPbI_3$ at different temperatures as well as an estimate of the binding energy of an exciton from the absorption profile were reported by Ruf et al.[21] These authors concluded that the E-A spectra resulted from the excitonic nature of the absorption caused by bound electron−hole pairs rather than unbound continuum states, consistent with our conclusion. Regarding the band profile of the E-A spectra, "a first derivative-like functional form" of the total absorption spectra was stated to reproduce the observed E-A spectra, in contrast with our conclusion. If the E-A spectra arise from only the exciton absorption of bound electron−hole pairs, the E-A spectra should be analyzed according to the derivative shapes of only the exciton absorption band, as described in our previous paper.[20] In the present work, we recorded the E-A spectra of a $MAPbI_3$ nanocrystalline film at temperatures in the range 290−60 K, that is, in both the tetragonal and the orthorhombic phases, and analyzed them with an integral method, under the assumption that the observed E-A spectra represent a linear combination of the zeroth, first, and second derivatives of the exciton absorption bands. Based on these results, the magnitudes of the change in the electric dipole moment and polarizability following photoexcitation into the exciton absorption band have been determined at each temperature. Hereafter, the tetragonal phase and orthorhombic phase are written as the TT phase and the OR phase, respectively, and integral method analysis is written as the I-M analysis.

The binding energy (19 meV) of an exciton estimated by Ruf et al.[21] from the simulation of the absorption profiles near 295 K is larger than the value reported in our previous paper (11.5 meV),[20] although both estimates were based on the E-A measurements. From the viewpoint of practical devices, e.g., in solar cells, where even a difference of 0.1% in efficiency has very important significance, the above-mentioned difference in binding energy is critical, and the problem must be solved. In the present work, we have evaluated the binding energy at different temperatures, based on a simulation of the absorption profiles which were assumed to be a sum of the exciton and continuum absorption profiles, each of which was obtained with the I-M analysis of the E-A spectra.

The reported exciton binding energy of $MAPbI_3$ in a range 2−85 meV was determined with the following methods: (1) a simulation of the absorption profile composed of an exciton band originating from the bound electron−hole pairs and continuum band resulting from a transition of an electron to the conduction band from the valence band;[17,20,21,28−34] (2) the temperature dependence of the photoluminescence (PL) intensity;[35−39] (3) the temperature dependence of the linewidth of the absorption profile;[40] (4) magneto-optical spectra;[41−45] and (5) static dielectric constant.[46] Each reported binding energy was estimated with one such method, but there is great variability among the values reported for $MAPbI_3$, as mentioned above. The exciton binding energy and photovoltaic behavior of perovskites depend on the fabrication and the film microstructure.[47] For this reason, it is unclear if the variability of the reported binding energy arises from the sample condition or from the estimation method. It is thus important to examine whether the above-mentioned methods give the same value of the binding energy for samples fabricated with the same procedure.

The I-M analysis of the E-A spectra yields a peak position and a linewidth of the exciton absorption bands.[20,23] Further, we could compare the exciton binding energy in the procedures (1) and (3) above, both in the TT phase and in the OR phase. For the $MAPbI_3$ nanocrystalline films prepared by the same fabrication, temperature-dependent PL spectra have been also measured, which allows a comparison of the binding energy for procedures (1)−(3). The binding energies estimated from the temperature-dependent absorption and the E-A spectra and temperature-dependent PL spectra have hence been compared for $MAPbI_3$ nanocrystalline films prepared with the same method, and with values reported so far for the $MAPbI_3$ solid films.

EXPERIMENTAL SECTION

Sample Preparation. MAI (homemade) and PbI_2 (molar ratio 1:1) powders were mixed in anhydrous DMF with a concentration of 45 mass % and stirred for 12 h at 70 °C in the nitrogen-purged glovebox to prepare the $MAPbI_3$ precursor solution. For the deposition of the $MAPbI_3$ layer, a suitable amount of $MAPbI_3$ precursor solution was dropped onto a fluorine-doped tin oxide (FTO)-coated glass substrate (spin-coating method, 5000 rpm for 15 s). After 5 s of spinning, chlorobenzene as an antisolvent was injected directly on the center of the substrate for rapid nucleation. The substrates were then annealed at 100 °C for 10 min. The morphology and thickness of the fabricated $MAPbI_3$ layer are shown in Figure 1, which shows an average grain size of about 1 μm of a prepared $MAPbI_3$ layer and a thickness of about 516 nm.

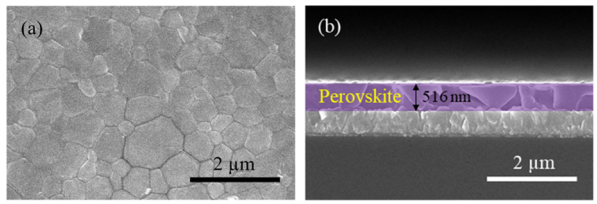

Figure 1. SEM images: (a) top view and (b) cross-sectional view of our $MAPbI_3$ film.

After the deposition of the $MAPbI_3$ layer onto the FTO-coated substrate, a thin poly(methyl methacrylate) (PMMA) film was spin-coated as an insulator, which also isolated the $MAPbI_3$ layer from the external environment (oxygen and moisture). A semitransparent layer of aluminum (Al) of thickness ∼15 nm was deposited by thermal evaporation on the sample substrates having a PMMA film on the perovskite layer. The FTO and Al films were used as electrodes; field strength was determined to be the applied voltage divided by the distance between the two films.

Measurements of Absorption, E-A, and PL Spectra at Different Temperatures. Optical spectra at various temperatures were measured under vacuum conditions with a cryogenic refrigerating system (Daikin, V202C5LR), equipped with silica optical

https://dx.doi.org/10.1021/acsaem.0c01983
ACS Appl. Energy Mater. 2020, 3, 11830−11840

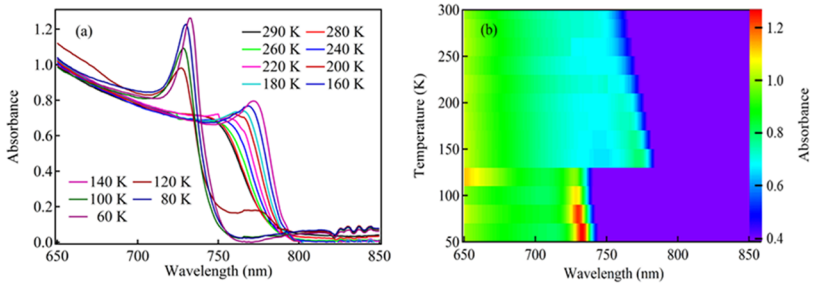

Figure 2. (a) Absorption spectra of the $MAPbI_3$ film observed at different temperatures. (b) T(temperature)-resolved absorption intensity image.

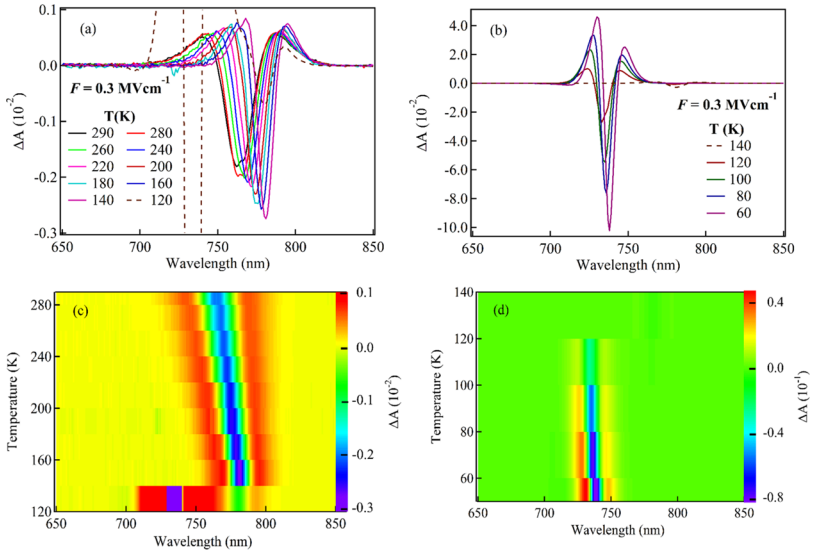

Figure 3. (a, b) E-A spectra of the $MAPbI_3$ film observed at different temperatures with $\boldsymbol{F}$ having a strength of 0.3 MV cm^{-1} for the TT and OR phases, respectively. (c, d) Temperature-resolved E-A images for the TT and OR phases, respectively.

windows, temperature controller (Scientific Inst., model 9600-1), and silicon diode thermometer. Absorption and PL spectra were measured with a commercially available spectrometer (JASCO, FP-777). An ac field with a modulation frequency of 40 Hz was applied for the measurements of the E-A spectra, with apparatus as described elsewhere.[48] Hereafter, the applied electric field is denoted by $\boldsymbol{F}$. The transmitted light intensity (T_{EX}) was modulated with a sinusoidal ac voltage applied between two electrodes of the samples with a function generator. A field-induced change in the transmitted light intensity (ΔT_{EX}) was measured at twice the modulation frequency ($2f$) with a lock-in amplifier. The dc component of T_{EX} was concurrently recorded with a computer. Plotting the field-induced change in absorbance $\Delta A\left(\equiv -\left(\frac{2\sqrt{2}}{\ln 10}\right)\left(\frac{\Delta T_{EX}(2f)}{T_{EX}}\right)\right)$ as a function of wavelength or wavenumber produced the E-A spectra.

RESULTS AND DISCUSSION

Absorption and E-A Spectra. Absorption spectra of the $MAPbI_3$ films were measured at different temperatures in the range 60−290 K. The results are shown in Figure 2, together with the temperature-resolved, i.e., T-resolved, absorption intensity image. The exciton band, which overlaps with a continuum band, showed a gradual red-shift from 750 to 772 nm, as the temperature decreased from 290 to 140 K; at the latter temperature, the crystal structure is assigned to the TT phase according to the XRD pattern (Supporting Information, SI, Figure S1). At 120 K, a second peak appeared at 730 nm besides the first peak at 773 nm, which indicates a mixture of the TT and OR phases. Upon further decreasing temperature, the intensity of the second peak, which corresponds to the OR phase, increased; this peak showed a monotonic red-shift, while the first peak that corresponds to the TT phase disappeared. The excitonic absorption band narrowed, as the temperature decreased (see Figure 2). A red-shift of the absorption band with decreasing temperature is commonly observed in lead-composite semiconductors, which is contrary to the Varshni trend because of the positive thermal-expansion coefficient of the band gap.[40,49]

Figure 3 shows the E-A spectra observed at different temperatures and their intensity image of $MAPbI_3$ in the TT and OR phases obtained at $2f$ of the modulated $\boldsymbol{F}$ with a strength of 0.3 MV cm^{-1}. Under the application of $\boldsymbol{F}$, a derivative shape was observed at each temperature around the exciton absorption band. The observed E-A spectra depend strongly on temperature (T); the intensity of the E-A signal increased monotonically, as T decreased. At 120 K, at which the crystal is a mixture of the TT and OR phases, the bands corresponding to these two phases show a concurrent field-induced change. Under the application of $\boldsymbol{F}$, semiconductors typically show the FKA effect, resulting from a field-induced modification of the continuum band, but the field-induced change in the absorption spectra of the $MAPbI_3$ nanocrystalline film observed in the present study is considered to result from only the field effect on the exciton absorption band at any temperature, as mentioned below in detail.

The E-A spectra of $MAPbI_3$ at different temperatures were reported by Ruf et al.;[21] the E-A signal was detected at the

https://dx.doi.org/10.1021/acsaem.0c01983
ACS Appl. Energy Mater. 2020, 3, 11830−11840

fundamental frequency (1*f*) and 2*f* of ***F***, but it is unclear whether the reported E-A spectra were measured at 1*f* or 2*f*. As we reported,[50] the exciton band of the $MAPbI_3$ film shows an electric-field-induced spectral broadening and narrowing, depending on the polarity of ***F***, which was detected on monitoring the E-A signals at 1*f*. This behavior depends on the sample condition, i.e., a strong 1*f* E-A signal was observed for the $MAPbI_3$ film sandwiched between FTO and PMMA films, whereas the 1*f* E-A signal was weak or negligible for the $MAPbI_3$ film sandwiched between TiO_2 and PMMA films. These 1*f* E-A signals are considered to originate as a result of interfacial interaction between the $MAPbI_3$ film and the conducting film of FTO. In contrast with the 1*f* signal, 2*f* E-A signals correspond to the bulk property; similar E-A spectra were observed for both the $MAPbI_3$ films sandwiched between FTO and PMMA films and between TiO_2 and PMMA films. In the present work, we have focused on the bulk property of the $MAPbI_3$ film; the E-A spectra in Figure 3 were recorded on detecting 2*f* signals at temperatures in the range 60−290 K. The E-A spectra observed with varied applied field strength at 60 and 290 K are shown in Figure 4. Plots of the E-A signal,

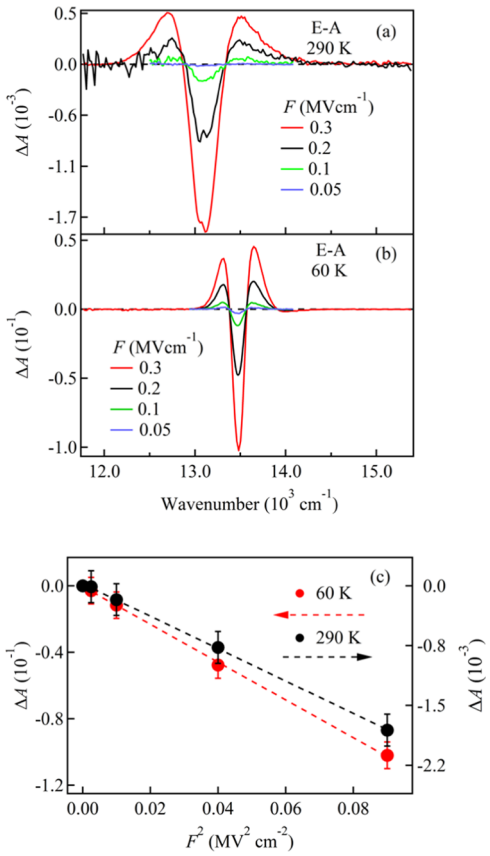

Figure 4. (a, b) E-A spectra of $MAPbI_3$ observed at 290 and 60 K, respectively, in the region of the exciton absorption band. (c) Plots of the change in the absorbance (ΔA) measured at the minimum as a function of the square of the applied field strength at 60 and 290 K.

which was monitored at the minimum, i.e., 13 547 cm^{-1} at 60 K and 13 111 cm^{-1} at 290 K, as a function of the applied field strength show that the E-A intensity is proportional to the square of the applied field strength at both 290 and 60 K, i.e., for both TT and OR phases. Then, it is known that the E-A signals of the $MAPbI_3$ nanocrystalline films are caused by the quadratic Stark effect, which then serves as a basis of the I-M analysis. As mentioned later, the exciton binding energy is estimated to be 11.6 and 24.2 meV in the TT and OR phases, respectively. Even with such low binding energy, the field-induced FKA oscillation, which is usually observed at the edge of the continuum absorption band, was not confirmed. This may be due to the lack of homogeneity and/or increased disorder caused by thermal fluctuation even at 60 K, which was the lowest temperature used in the present experiments.

Theoretical Background and Analysis of the E-A Spectra. The Stark effect shifts the energy of the absorption band by $-\Delta\boldsymbol{\mu}\boldsymbol{F} - \Delta\boldsymbol{\alpha}\boldsymbol{F}^2/2$ in the presence of ***F***; $\Delta\boldsymbol{\mu}$ and $\Delta\boldsymbol{\alpha}$ represent the change in the electric dipole moment and polarizability, respectively, following photoexcitation, i.e., the difference between the excited state (e) and ground state (g), that is, $\Delta\boldsymbol{\mu} = \boldsymbol{\mu}_e - \boldsymbol{\mu}_g$ and $\Delta\boldsymbol{\alpha} = \boldsymbol{\alpha}_e - \boldsymbol{\alpha}_g$. The field-induced change in absorbance at wavenumber ν, that is, $\Delta A(\nu)$, is given by a sum of the zeroth, first, and second derivatives of absorbance $A(\nu)$,[51−54]

$$\Delta A(\nu) = (fF)^2\left[\alpha_\chi A(\nu) + \beta_\chi \nu \frac{\mathrm{d}}{\mathrm{d}\nu}\left(\frac{A(\nu)}{\nu}\right) + \gamma_\chi \nu \frac{\mathrm{d}^2}{\mathrm{d}\nu^2}\left(\frac{A(\nu)}{\nu}\right)\right] \quad (1)$$

where f is the internal field factor and $F = |\boldsymbol{F}|$. Each of α_χ, β_χ, and γ_χ corresponds to the change in absorption intensity, spectral shift, and broadening of the absorption spectrum, respectively. The magnitudes of $\Delta\boldsymbol{\mu}$ and $\Delta\boldsymbol{\alpha}$ were calculated by β_χ and γ_χ, which could be given at a magic angle χ, that is, 54.7° as follows

$$\beta_\chi = \frac{\Delta\bar{\alpha}}{2hc}, \gamma_\chi = \frac{|\Delta\mu|^2}{6h^2c^2} \quad (2)$$

where $\Delta\bar{\alpha}$ denotes the trace of $\Delta\boldsymbol{\alpha}$.

Exciton and continuum absorption bands of $MAPbI_3$ overlap severely, and the separation of these bands is difficult. In such a case, an integral method is useful to analyze the E-A spectrum.[55] If the E-A spectrum is expressed with eq 1, the first and second integrals of the E-A spectrum over the wavenumber are given as follows

$$\int \Delta A(\nu) \cong (fF)^2\left[\alpha_\chi \int A(\nu)\mathrm{d}\nu + \beta_\chi A(\nu) + \gamma_\chi \frac{\mathrm{d}A(\nu)}{\mathrm{d}\nu}\right] \quad (3)$$

$$\int\left\{\int \Delta A(\nu)\mathrm{d}\nu\right\} \cong (fF)^2\left[\alpha_\chi \int\left\{\int A(\nu)\mathrm{d}\nu\right\}\mathrm{d}\nu + \beta_\chi \int A(\nu)\mathrm{d}\nu + \gamma_\chi A(\nu)\right] \quad (4)$$

Estimation of $\Delta\mu$ and $\Delta\bar{\alpha}$. The values of α_χ, β_χ, and γ_χ in eqs 1−4 could be obtained by simulating E-A spectra and their first and second integral spectra. Figure 5 shows the results for the E-A spectra observed at 290, 120, and 60 K. The results for E-A spectra at other temperatures are shown in Figures S2−S5 of the SI. The magnitudes of $|\Delta\mu|$ and $\Delta\bar{\alpha}$ shown in Figure 6 have been evaluated at each temperature with γ_χ and β_χ, respectively, using eq 2. Note that the values of $|\Delta\mu|$ and $\Delta\bar{\alpha}$ estimated at each temperature from the I-M analysis are listed

https://dx.doi.org/10.1021/acsaem.0c01983
ACS Appl. Energy Mater. 2020, 3, 11830−11840

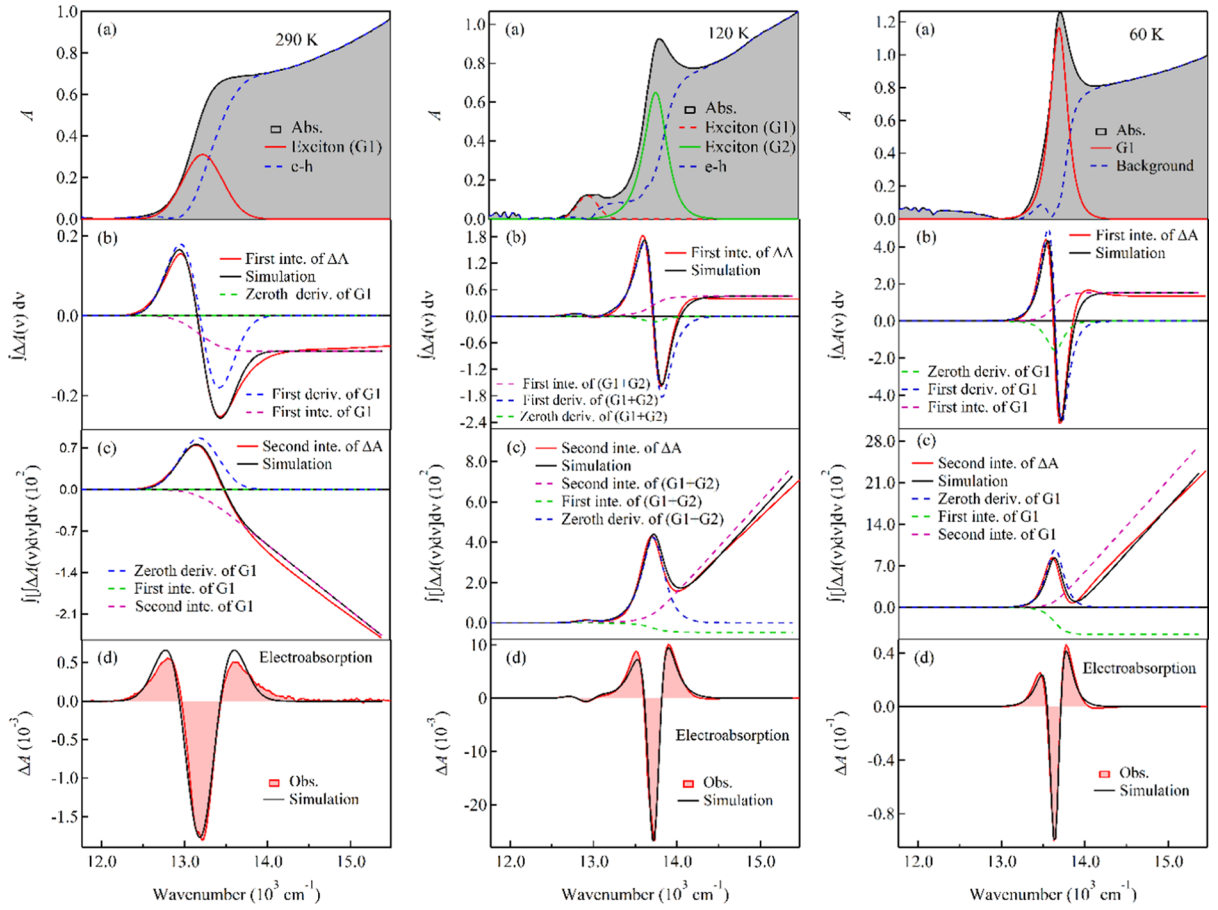

Figure 5. I-M analysis of the E-A spectra of $MAPbI_3$ at 290, 120, and 60 K (from left to right). (a) Absorption spectrum, (b, c) first and second integrals of the E-A spectrum, respectively, and (d) E-A and simulated spectra.

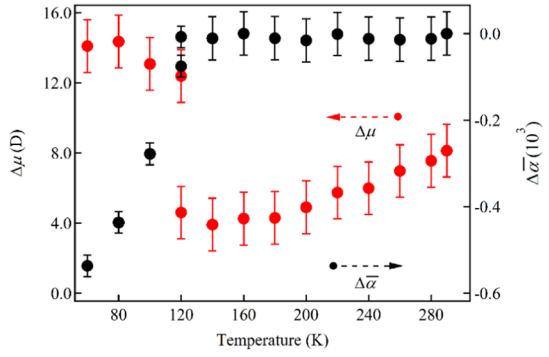

Figure 6. Plots of $|\Delta\mu|$ (red circle) and $\Delta\bar{\alpha}$ (black circle) following the exciton absorption of the $MAPbI_3$ polycrystalline film against temperature. See text for the evaluation method.

in SI (Table S1). At 290 K, the value of $|\Delta\mu|$ was ~8.14 D, and $\Delta\bar{\alpha}$ was negligibly small. As the temperature decreased, the value of $|\Delta\mu|$ gradually decreased, whereas the magnitude of $\Delta\bar{\alpha}$ was small and remained constant up to 140 K. At 120 K, at which both TT and OR phases coexist, the values of $|\Delta\mu|$ and $\Delta\bar{\alpha}$ were 4.6 ± 1.5 D and −7.5 ± 25 Å^3, respectively, in the TT phase and 12.4 ± 1.5 D and −75 ± 25 Å^3, respectively, in the OR phase. As the temperature decreased from 120 K, i.e., in the OR phase, the magnitudes of both $|\Delta\mu|$ and $\Delta\bar{\alpha}$ increased and reached 14.1 ± 1.5 D and −536 ± 25 Å^3, respectively, at 60 K. The peak position ($h\nu_0$) and linewidth (FWHM) of the exciton absorption band at each temperature, which were determined with the I-M analysis of the E-A spectra, are shown in the SI (Table S2). The present value of $|\Delta\mu|$ at room temperature is larger than that reported previously,[20] i.e., 2.4 D, estimated with the same method of analysis, which is attributed to a larger crystal size of $MAPbI_3$ in the present work, which is also responsible for improving the efficiency of conversion of photons to energy in a solar cell.[56,57] In the analysis of the E-A spectra, only the absolute value could be determined for $\Delta\mu$, and it is not clear whether the electric dipole moment increased or decreased on photoexcitation. As mentioned later, the PL spectra of exciton showed a remarkable red-shift, relative to the absorption band, suggesting that the magnitude of the electric dipole moment increases with photoexcitation into the exciton band. The negative values of $\Delta\bar{\alpha}$ indicate that the magnitude of the polarizability in this material is larger in the ground state than in the exciton state. The magnitude of $\Delta\bar{\alpha}$ in the OR phase is much larger than that in the TT phase, implying that the polarizability of the $MAPbI_3$ film in the ground state is much larger in the OR phase than that in the TT phase. The significant blue shift of the exciton absorption band following phase transition from the TT phase to the OR phase may be related to the big difference in the polarizability of the ground state between these two phases (see Figure 2).

Estimation of Exciton Binding Energy. The values of the exciton binding energy (E_B) at each temperature can be estimated from the Elliott fit of the absorption spectra,[58] on assuming a Gaussian shape for the exciton and remaining

https://dx.doi.org/10.1021/acsaem.0c01983
ACS Appl. Energy Mater. 2020, 3, 11830−11840

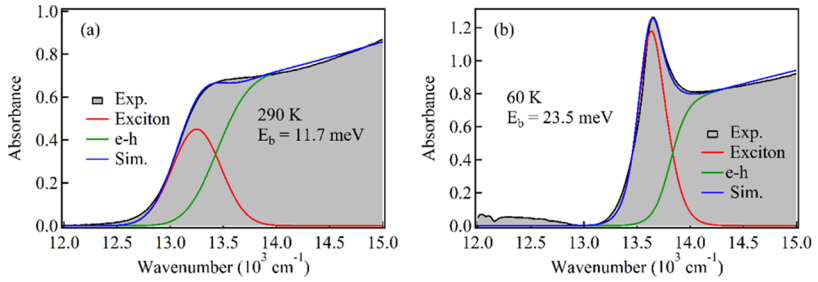

Figure 7. Absorption spectra of the $MAPbI_3$ film at 290 K (a) and 60 K (b). The shaded areas show the observed spectra; a blue line shows the spectrum simulated as a sum of the exciton band (red) and continuum band (green). See Table S2 for the parameters used in the simulation.

continuum bands. The absorbance at the angular frequency (ω) can be given by the following equation[20]

$$A(\omega) = C_{ex}\sum_{n}\frac{\sqrt{E_B}}{n^3}G^{ex}(\omega) + C_{e-h}\sum_{k=0}^{Z_{end}/h}G^{cont}(\omega) \times \frac{2\pi\sqrt{E_B}}{1 - e^{-2\pi(\sqrt{2\beta}\sqrt{E_B}/\sqrt{1-\sqrt{1-4\beta(Z_k-E_g)}})}} \frac{1}{\sqrt{1 - 4\beta(Z_k-E_g)}} \quad (5)$$

in which

$$G^{ex}(\omega) = e^{-((\hbar\omega-(E_g-(E_B/n^2)))^2/2\sigma^2)}$$

$$G^{cont}(\omega) = e^{-((\hbar\omega-Z_k)^2/2\sigma^2)}$$

In eq 5, the first and second terms correspond to the exciton and continuum bands, respectively; Z_k is the kth dummy variable that has equal space in wavenumber ~0.81 cm^{-1}; β represents the magnitude of the nonparabolicity of the band dispersion; E_g is the band gap energy; the relation $E_g = \hbar\nu_0 + E_B$ holds. Here, $\hbar\nu_0$ is the energy of the exciton band. Gaussian functions were assumed for G^{ex} to analyze the E-A spectra. σ in eq 5 was determined from the linewidth of the exciton band. As already mentioned, only the exciton band showed the electric field effect, and the value of full width at half-maximum (FWHM) extracted from the E-A spectra was used as a linewidth of the exciton absorption band. Absorption spectra, simulated as a combination of exciton and continuum bands, have been reproduced satisfactorily with eq 5. The parameters E_B, β, and C_{ex}/C_{e-h} used in the simulation are listed in SI (Table S2). Figure 7 shows the results at 290 and 60 K. The results at other temperatures are shown in the SI (Figures S6 and S7). Then, the average value of E_B was evaluated to be 11.6 meV in the TT phase and 24.2 meV in the OR phase; E_B is known to be independent of temperature in each of the TT and OR phases. E_B in the OR phase estimated at 120 K, at which the exciton absorption bands in both TT and OR phases were observed, was much smaller than the other values in the OR phase (see Figure S6 of the SI); this value at 120 K was excluded from a calculation of the average value.

The value of E_B was estimated also using the linewidths of the temperature-dependent absorption band obtained through the I-M analysis of the E-A spectra (see Table S2 of the SI), as reported by D'Innocenzo et al.[40] A temperature-dependent exciton linewidth in a semiconductor at temperature T, $\Gamma(T)$, is related to an exciton−phonon interaction and given by[59]

$$\Gamma(T) = \Gamma_0 + \gamma T + \Gamma_B N_{LO}(T) \quad (6)$$

The first term on the right-hand side corresponds to the temperature-independent inhomogeneous broadening, which arises from scattering due to impurities and imperfections. The second and third terms result from the exciton interactions with acoustic phonon and LO phonon, respectively. γ and Γ_B are the exciton−acoustic phonon and exciton−LO phonon coupling strength, respectively; $N_{LO}(T)$ is given by the Bose function, i.e., $1/[\exp(E_{LO}/k_BT) - 1]$, with phonon energy E_{LO} and Boltzmann constant k_B. LO phonons might scatter excitons to bound states and continuum states. On assuming that interactions of excitons with LO phonons predominantly lead to exciton dissociation, the relation between $\Gamma(T)$ and E_B is

$$\Gamma(T) = \Gamma_0 + \gamma T + \frac{\Gamma_B}{e^{E_B/k_BT} - 1} \quad (7)$$

On neglecting γT in eq 6 and assuming $E_{LO} \gg k_BT$, i.e., $E_B \gg k_BT$, eq 7 becomes similar to the relation used by D'Innocenzo et al.[40] to estimate E_B of $MAPbI_3$ from $\Gamma(T)$ of the exciton absorption band. The value of $\Gamma(T)$ of the $MAPbI_3$ film, i.e., FWHM, evaluated with the I-M analysis of the E-A spectra, was plotted as a function of the inverse of temperature. The plots were simulated well with eq 7, as shown in Figure 8, with

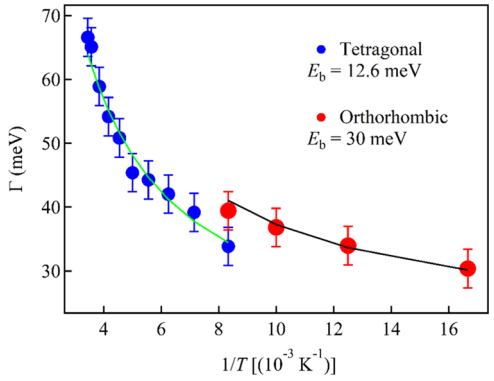

Figure 8. Plots of the linewidth of the exciton absorption band of the $MAPbI_3$ film as a function of the inverse of temperature.

the values of Γ_0, γ, and Γ_B given in Table 1; E_B is estimated to be 12.6 meV in the TT phase and 30 meV in the OR phase. These values are a little larger than the average value estimated from the simulation of the absorption profile, i.e., 11.6 and 24.2 meV, respectively. However, the fact that the simulation of the absorption profile and temperature-dependent linewidth of the exciton absorption band give quite similar values for the binding energy of the exciton may indicate that the exciton scattering by LO phonons leads predominantly to exciton

https://dx.doi.org/10.1021/acsaem.0c01983
ACS Appl. Energy Mater. 2020, 3, 11830−11840

Table 1. Magnitude of Parameters Γ_0, Γ_B, and γ Used for Simulation of the Temperature-Dependent Linewidths of the Exciton Absorption Band to Evaluate E_B in the Tetragonal (TT) and Orthorhombic (OR) Phases with eq 7

	tetragonal (TT)	orthorhombic (OR)
Γ_0 (meV)	20	20
Γ_B (meV)	17.8	15
γ (meV K^{-1})	0.058	0.168

dissociation. The importance of the exciton−LO phonon interaction in the dissociation of an exciton might indicate the significance of a polaron effect,[11,31] which arises from the Coulomb interaction between carriers and ionic lattice, as the origin of slow carrier mobility. In the present results, the exciton−acoustic phonon interaction is much larger in the OR phase than in the TT phase, i.e., γ in eqs 6 and 7, as shown in Table 1. This result might be related to the fact that trap emission relative to exciton emission is much larger in the OR phase than in the TT phase, as shown later.

Temperature-Dependent PL Spectra and Estimation of Binding Energy. The PL spectra of the $MAPbI_3$ films were recorded at different temperatures in the range 60−290 K; the PL spectra appear in Figure 9a, with the temperature-resolved intensity image (Figure 9b). A clear exciton emission was observed at high temperatures. In the temperature range in which the crystal structure is assigned to the TT phase, the peak of the exciton emission spectra shows a red-shift with decreasing temperature, that is, the maximum intensity was at 768 and 790 nm at 290 and 140 K, respectively. As the temperature decreased below 120 K, at which the crystal structure was assigned to the OR phase (see Figure S1), the peak of the exciton emission showed a blue shift and its intensity rapidly decreased; a new band appeared with a peak at 840 nm, which was assigned to trap emission. It has been reported[60] that a minor volume fraction of the TT phase coexists at low temperatures with the dominant OR phase in $MAPbI_3$ polycrystalline films and that the PL originating from the TT phase following charge transfer from the OR phase appears, besides the emissions originating from the OR phase and trap states. Then, it may be important to note that the emission intensity data at temperatures above 160 K, where only the TT phase exists, is included in Figure 9c.

As a relaxation from the exciton state in the TT phase, radiative process to give PL, nonradiative thermal process to the ground state, energy transfer to trap states including impurities or defects in crystals and dissociation process to produce electron and hole are considered. Among these processes, energy transfer to the trap states, which is considered to depend on temperature because of the remarkable temperature dependence of the trap emission intensity, might be neglected in the tetragonal phase, in which the exciton emission is dominant and trap emission is negligible. If only the exciton dissociation process depends on the temperature in the TT phase, the rate constant for the decay of exciton (k_{ex}) is expressible as $k_{ex} = k^r + k^{nr} + k_{dis} \exp(-E_B/k_BT)$, where k^r, k^{nr}, and k_{dis} represent radiative and nonradiative decay rate constants and dissociation rate constant, respectively. Both k^r and k^{nr} are assumed to be independent of temperature. Under such conditions, E_B in the TT phase may be estimated from the plots of PL intensity as a function of temperature.

The PL quantum yield at temperature T, $\Psi(T)$, is given by k^r/k_{ex}, and $1/\Psi(T)$ is given as follows

$$\frac{1}{\Psi(T)} = \frac{1}{\Psi(T=0)} + \frac{k_{dis}}{k^r}\exp\left(-\frac{E_B}{k_BT}\right) \quad (8)$$

Here, $\Psi(T = 0) = k^r/(k^r + k^{nr})$. The value of E_B is then determined on fitting $I(T)$, the PL intensity, with the following equation

$$\frac{1}{I(T)} = C_1 + C_2\exp\left(-\frac{E_B}{k_BT}\right) \quad (9)$$

in which C_1 and C_2 are fitting parameters and C_1 corresponds to the inverse of $I(T)$ at $T = 0$ K. Several authors reported the value of E_B of $MAPbI_3$ determined with eq 9. The present temperature-dependent $I(T)$ in the temperature range 160−290 K is also well-fitted with eq 9, as shown in Figure 9c. E_B is

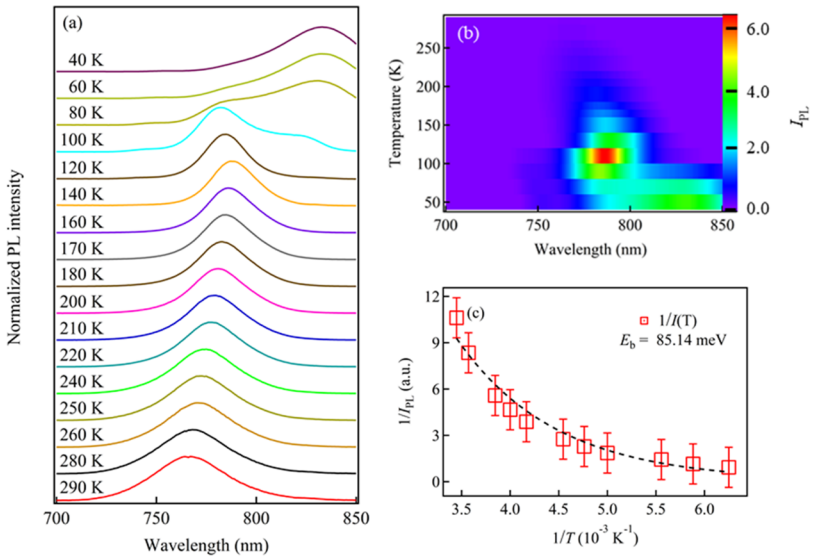

Figure 9. (a) PL spectra of the $MAPbI_3$ film at various temperatures (T = 40−290 K), (b) T-resolved intensity image of PL spectra, and (c) inverse of PL intensity of the $MAPbI_3$ film as a function of the inverse of T from 160 to 290 K.

https://dx.doi.org/10.1021/acsaem.0c01983
ACS Appl. Energy Mater. 2020, 3, 11830−11840

then estimated to be 85 ± 30 meV, which is about 10 times the value of E_B determined from fitting the absorption profile in the TT phase. The large difference in the binding energies estimated from the two processes suggests that the exciton produced directly by photoirradiation and the exciton that emits PL are very different from each other, as we suggested earlier for $MAPbBr_3$ quantum dots.[23] It was also suggested that the analysis using PL measurement might overestimate the exciton binding energy because of the existence of nonradiative recombination process.[61]

As already mentioned, the unique structure and associated dielectric responses in halide perovskites including $MAPbI_3$ have led to the proposal of large polaron formation having strong electron−phonon coupling.[11,31,62] As shown in the SI (Figure S8), the peak position of the PL spectra shows a red-shift, relative to the exciton absorption peak, e.g., the shift is ∼180 and ∼190 cm^{-1} at 290 and 200 K, respectively. As shown in Figure S8 of the SI, further, the spectral width of the PL band in the TT phase, which monotonically decreased with decreasing temperature, is larger than that of the exciton absorption band by 160 ± 30 cm^{-1} at each temperature, e.g., the linewidths of the PL band were 720 and 530 cm^{-1} at 290 and 200 K, respectively, which are very similar to the ones reported so far.[63] Note that the peak position and linewidth of the exciton absorption band at each temperature is shown in Table S2. These spectral shift and broadening of the PL spectra, in comparison with the exciton absorption spectrum, may result from the polaron formation, indicating the polar nature and strong electron−phonon coupling in the $MAPbI_3$ solid films.

Comparison of the Present Binding Energy of the $MAPbI_3$ Film with the Reported Values. The efficiency of photovoltaic cells constructed with the $MAPbI_3$ film depends on the sample condition including the microstructure of the $MAPbI_3$ film.[46] The binding energy (E_B) is then expected to show a variation among experiments in which E_B was estimated, as the fabrications of the $MAPbI_3$ films and the sample conditions of the crystal might differ. Even so, a comparison of the E_B value estimated in the present results with other results reported so far might be important to an understanding of the intrinsic physical property of the exciton produced by photoirradiation of the $MAPbI_3$ polycrystalline film.

The E_B value estimated from fitting the absorption profile was reported to be 10 ± 5 meV at room temperature (TT phase) by seven groups including ours,[17,20,29−33] despite the varied fabrication method of the $MAPbI_3$ films. The value of E_B near 295 K estimated with magneto-optical measurements is also located in this region, i.e., ∼5 and ∼12 meV.[44,45] The present E_B value in the TT phase is hence consistent with the reported results, although greater binding energies, i.e., 19, 25, and 29 meV were also reported,[21,28,34] based on fitting the absorption profile, and a small value, 2 meV, was estimated from static dielectric constant.[46]

The E_B value in the OR phase at low temperatures estimated from fitting the absorption profile is larger than that in the TT phase when a comparison is made within the same research group; the magnitude of E_B was estimated to be in the range 15−34 meV.[21,29−31,33,34] The present value, i.e., 24.2 meV, is nearly in the middle of these reported values. In the magneto-optical experiments, the E_B value in the OR phase at low temperature was estimated to be 37, 50, and 16 meV;[41−45] the E_B values obtained in the TT phase by two groups were smaller than the ones in the OR phase,[44,45] consistent with the relation in E_B between the TT and OR phases, obtained from fitting the absorption profile, including the present result.

D'Innocenzo et al. estimated E_B to be 55 ± 20 meV in the TT phase with the temperature-dependent linewidth of the exciton absorption band ($\Gamma(T)$).[40] As mentioned already, it was assumed in their analysis that $\exp(-E_B/k_BT) \gg 1$ in eq 7, that is, E_B is much larger than k_BT; the contribution of the exciton−acoustic phonon interaction was not considered, and their value might be regarded as the upper estimate for the exciton binding energy.[64] As far as $\Gamma(T)$ values estimated from the I-M analysis of the E-A spectra are concerned, their assumption cannot be applied, as the magnitude of $\ln(\Gamma(T) - \nu_0)$ plotted as a function of inverse T deviates from a straight line. As already mentioned, the present E_B values estimated with eq 7 from the temperature-dependent $\Gamma(T)$, i.e., 12.6 and 30 meV, respectively, in the TT and OR phases, are near, but a little larger than the values evaluated from fitting the absorption profile, implying that a part of excitons interacting with LO phonons return to the bound state without dissociation.

In a single crystal of $MAPbI_3$, LO phonon energy, i.e., E_{LO}, was estimated to be 16.1 meV with the temperature-dependent spectral width of the photocurrent peak due to the exciton absorption of the OR phase, and the binding energy of free exciton was also derived to be 12.4 ± 1.2 meV at low temperatures, i.e., in the OR phase, based on the estimation of the photocurrent caused by exciton dissociation into free carriers under exciton-resonant excitation.[61] Thus, the binding energy of exciton in the single crystal of $MAPbI_3$ was shown to be smaller than the LO phonon energy by 3.7 meV, which is similar to the present results of the $MAPbI_3$ polycrystalline film. The result that the binding energy of $MAPbI_3$ is larger in polycrystalline films than that in single crystal may be caused by the influence of grain structures, that is, polycrystalline film may be quite sensitive to the surrounding external force.[60] There is another report that the exciton binding energy and reduced mass of carriers remain effectively unchanged with grain size,[65] which was examined at 2 K, i.e., under the condition where thermal fluctuations of the interactions were frozen and the rotational disorder of the organic cation was negligible. In temperatures at which practical devices are used, however, there may be a possibility that the binding energy depends on the sample condition since dynamic disorder caused by orientation and mobility of the cation cannot be negligible in the crystals of $MAPbI_3$.[66] In the present sample condition, for example, the effect of thermal fluctuation and dynamic disorder may be unable to be excluded even at the lowest temperature of 60 K.

The present E_B value estimated from the PL intensity observed at different temperatures is much larger than both values evaluated from the absorption profile and evaluated from the temperature-dependent linewidth of the exciton absorption band. Similar results were also obtained for $MAPbBr_3$ quantum dots, of which the E_B value evaluated from the temperature-dependent PL intensity (∼70 meV) was much larger than the one evaluated from the exciton absorption profile (∼17 meV), as mentioned previously.[23] The E_B values of the $MAPbI_3$ film estimated by other groups from the PL intensity are also large, i.e., 68.3 and 83.2 meV,[38,39] compared with the E_B values estimated from the absorption profile. Sun et al.[35] and Savenije et al.[36] reported small E_B values, i.e., 19 ± 3 and 32 ± 5 meV, respectively,

https://dx.doi.org/10.1021/acsaem.0c01983
ACS Appl. Energy Mater. 2020, 3, 11830−11840

based on the PL intensity. In their plots of the PL intensity as a function of temperature, however, PL intensities observed in the temperature range from ∼80 to ∼300 K and from ∼10 to ∼300 K were used for simulation. $MAPbI_3$ crystals show a phase transition from the TT to OR phase, as the temperature decreases from 300 to 100 K; both the PL properties and XRD patterns change much across the phase transition (see Figures 9 and S1). As already mentioned, the TT and OR phases show disparate E_B values. The estimation from the PL intensity in the temperature range including both TT and OR phases is likely to mislead to incorrect binding energy of an exciton produced on the photoirradiation. As mentioned already and shown in Figure S8 of the SI; further, the PL peak shows a large red-shift, relative to the exciton absorption peak, and the PL band is much broader than the exciton absorption band, suggesting that the excitons produced by photoexcitation are very different from the excitons that give PL.

CONCLUSIONS

Electroabsorption (E-A) spectra of the $MAPbI_3$ nanocrystalline film detected at the second harmonic of the modulation frequency of the applied electric field have been interpreted in terms of a quadratic Stark effect on the exciton absorption band; an integral method has been applied to analyze the E-A spectra observed at temperatures in the range 60−290 K. The magnitudes of the change in electric dipole moment ($|\Delta\mu|$) and polarizability ($\Delta\bar{\alpha}$) following absorption into the exciton band have been evaluated at each temperature. A transition from the TT phase to the OR phase occurred at ∼120 K, as the temperature of the $MAPbI_3$ film decreased from 290 to 60 K; the temperature dependence of both $|\Delta\mu|$ and $\Delta\bar{\alpha}$ differs greatly in these TT and OR phases. An analysis of the E-A spectra yielded the peak position and the linewidth of the exciton absorption band, resulting in a clear separation between the exciton absorption band and continuum band, arising in a transition from the valence band to the conduction band. By fitting the total absorption spectra composed of exciton and continuum bands, the binding energy of exciton (E_B) is evaluated at each temperature, i.e., 11.6 meV in the TT phase and 24.2 meV in the OR phase on average, which are nearly independent of the temperature. With the temperature-dependent linewidth of the exciton absorption profile, which was determined through the I-M analysis of the E-A spectra at each temperature, E_B has been estimated to be 12.6 and 30 meV in TT and OR phases, respectively. These values are near, but a little larger than those evaluated from fitting the absorption profile, implying that some excitons interacting with LO phonons pass to the bound state without dissociation. The E_B value of the $MAPbI_3$ film was evaluated also from the temperature-dependent PL intensity to be 85 ± 30 meV in the TT phase. This value is much larger than the value evaluated from a simulation of the absorption profile or the temperature-dependent linewidth of the exciton absorption profile, even when a comparison is made among samples fabricated with the same procedure.

ASSOCIATED CONTENT

Supporting Information

The Supporting Information is available free of charge at https://pubs.acs.org/doi/10.1021/acsaem.0c01983.

XRD patterns, integral method analysis of the E-A spectra, simulation of absorption profiles, peak position, and bandwidth of the exciton absorption and PL bands as a function of temperature, magnitudes of the change in electric dipole moment and polarizability following exciton absorption at each temperature, and fitted parameters used for a theoretical simulation of optical transitions (PDF)

AUTHOR INFORMATION

Corresponding Author

Nobuhiro Ohta − *Department of Applied Chemistry and Institute of Molecular Science and Center for Emergent Functional Matter Science, National Chiao Tung University, Hsinchu 30010, Taiwan;* orcid.org/0000-0003-4255-6448; Email: nohta@nctu.edu.tw

Authors

Morihiko Hamada − *Department of Applied Chemistry and Institute of Molecular Science, National Chiao Tung University, Hsinchu 30010, Taiwan*

Shailesh Rana − *Department of Applied Chemistry and Institute of Molecular Science, National Chiao Tung University, Hsinchu 30010, Taiwan*

Efat Jokar − *Department of Applied Chemistry and Institute of Molecular Science and Center for Emergent Functional Matter Science, National Chiao Tung University, Hsinchu 30010, Taiwan*

Kamlesh Awasthi − *Department of Applied Chemistry and Institute of Molecular Science and Center for Emergent Functional Matter Science, National Chiao Tung University, Hsinchu 30010, Taiwan;* orcid.org/0000-0001-7852-059X

Eric Wei-Guang Diau − *Department of Applied Chemistry and Institute of Molecular Science and Center for Emergent Functional Matter Science, National Chiao Tung University, Hsinchu 30010, Taiwan;* orcid.org/0000-0001-6113-5679

Complete contact information is available at: https://pubs.acs.org/10.1021/acsaem.0c01983

Author Contributions

§M.H. and S.R. contributed equally to this work.

Notes

The authors declare no competing financial interest.

ACKNOWLEDGMENTS

Taiwan Ministry of Science and Technology (MOST 108-2113-M-009-002, MOST 108-2811-M-009-509, MOST 108-2119-M-009-004, and MOST 109-2634-F-009-028) and the Center for Emergent Functional Matter Science of National Chiao Tung University from The Featured Areas Research Center Program within the framework of the Higher Education Sprout Project by Taiwan Ministry of Education (MOE) supported this work.

REFERENCES

(1) Jena, A. K.; Kulkarni, A.; Miyasaka, T. Halaide Perovskite Photovoltaics: Background, Status, and Future Prospect. *Chem. Rev.* **2019**, *119*, 3036−3103.

(2) Green, M. A.; Ho-Baillie, A.; Snaith, H. J. The Emergence of Perovskite Solar Cells. *Nat. Photonics* **2014**, *8*, 506−514.

(3) Yoo, E. J.; Lyu, M.; Yun, J. H.; Kang, C. J.; Choi, Y. J.; Wang, L. Resistive Switching Behavior in Organic-Inorganic Hybrid

$CH_3NH_3PbI_3$-XClx Perovskite for Resistive Random Access Memory Devices. *Adv. Mater.* **2015**, *27*, 6170−6175.
(4) Stranks, S. D.; Eperon, G. E.; Grancini, G.; Menelaou, C.; Alcocer, M. J. P.; Leijtens, T.; Herz, L. M.; Petrozza, A.; Snaith, H. J. Electron-Hole Diffusion Lengths Exceeding 1 Micrometer in an Organometal Trihalide Perovskite Absorber. *Science* **2013**, *342*, 341−345.
(5) Sutherland, B. R.; Sargent, E. H. Perovskite Photonic Sources. *Nat. Photonics* **2016**, *10*, 295−302.
(6) Hu, X.; Zhang, X.; Liang, L.; Bao, J.; Li, S.; Yang, W.; Xie, Y. High-Performance Flexible Broadband Photodetector Based on Organolead Halide Perovskite. *Adv. Funct. Mater.* **2014**, *24*, 7373−7380.
(7) Li, B.; Hui, W.; Ran, X.; Xia, Y.; Xia, F.; Chao, L.; Chen, Y.; Huang, W. Metal Halide Perovskites for Resistive Switching Memory Devices and Artificial Synapses. *J. Mater. Chem. C* **2019**, *7*, 7476−7493.
(8) Stranks, S. D.; Hoye, R. L. Z.; Di, D.; Friend, R. H.; Deschler, F. The Physics of Light Emission in Halide Perovskite Devices. *Adv. Mater.* **2019**, *31*, 1803336.
(9) Kulkarni, S. A.; Baikie, T.; Boix, P. P.; Yantara, N.; Mathews, N.; Mhaisalkar, S. Band-Gap Tuning of Lead Halide Perovskites Using a Sequential Deposition Process. *J. Mater. Chem. A* **2014**, *2*, 9221−9225.
(10) Oga, H.; Saeki, A.; Ogomi, Y.; Hayase, S.; Seki, S. Improved Understanding of the Electronic and Energetic Landscapes of Perovskite Solar Cells: High Local Charge Carrier Mobility, Reduced Recombination, and Extremely Shallow Traps. *J. Am. Chem. Soc.* **2014**, *136*, 13818−13825.
(11) Baranowski, M.; Plochocka, P. Excitons in Metal-Halide Perovskites. *Adv. Energy Mater.* **2020**, *10*, 1903659.
(12) Ohta, N.; Awasthi, K.; Okoshi, K.; Manseki, K.; Miura, H.; Inoue, Y.; Nakamura, K.; Kono, H.; Diau, E. W. G. Stark Spectroscopy of Absorption and Emission of Indoline Sensitizers: A Correlation with the Performance of Photovoltaic Cells. *J. Phys. Chem. C* **2016**, *120*, 26206−26216.
(13) Li, X.; Wang, X.; Zhang, W.; Wu, Y.; Gao, F.; Fang, J. The Effect of External Electric Field on the Performance of Perovskite Solar Cells. *Org. Electron.* **2015**, *18*, 107−112.
(14) Yu, X.; Yang, L.; Lv, Q.; Xu, M.; Chen, H.; Yang, D. The Enhanced Effiiciency of Graphene-Silicon Solar Cells by Electric Field Doping. *Nanoscale* **2015**, *7*, 7072−7077.
(15) Roiati, V.; Mosconi, E.; Listorti, A.; Colella, S.; Gigli, G.; De Angelis, F. Stark Effect in Perovskite/TiO_2 Solar Cells: Evidence of Local Interfacial Order. *Nano Lett.* **2014**, *14*, 2168−2174.
(16) Wu, X.; Yu, H.; Li, N.; Wang, F.; Xu, H.; Zhao, N. Composition-Dependent Light-Induced Dipole Moment Change in Organometal Halide Perovskites. *J. Phys. Chem. C* **2015**, *119*, 1253−1259.
(17) Ziffer, M. E.; Mohammed, J. C.; Ginger, D. S. Electroabsorption Spectroscopy Measurements of the Exciton Binding Energy, Electron-Hole Reduced Effective Mass, and Band Gap in the Perovskite $CH_3NH_3PbI_3$. *ACS Photonics* **2016**, *3*, 1060−1068.
(18) Amerling, E.; Baniya, S.; Lafalce, E.; Zhang, C.; Vardeny, Z. V.; Whittaker-Brooks, L. Electroabsorption Spectroscopy Studies of $(C_4H_9NH_3)_2PbI_4$ Organic-Inorganic Hybrid Perovskite Multiple Quantum Wells. *J. Phys. Chem. Lett.* **2017**, *8*, 4557−4564.
(19) Awasthi, K.; Wang, C.-Y.; Fathi, A.; Narra, S.; Diau, E. W.-G.; Ohta, N. Anisotropic Electric Field Effect on the Photoluminescence of $CH_3NH_3PbI_3$ Perovskite Sandwiched between Conducting and Insulating Film. *J. Phys. Chem. C* **2017**, *121*, 22700−22706.
(20) Awasthi, K.; Du, K. B.; Wang, C. Y.; Tsai, C. L.; Hamada, M.; Narra, S.; Diau, E. W. G.; Ohta, N. Electroabsorption Studies of Multicolored Lead Halide Perovskite Nanocrystalline Solid Films. *ACS Photonics* **2018**, *5*, 2408−2417.
(21) Ruf, F.; Magin, A.; Schultes, M.; Ahlswede, E.; Kalt, H.; Hetterich, M. Excitonic Nature of Optical Transitions in Electroabsorption Spectra of Perovskite Solar Cells. *Appl. Phys. Lett.* **2018**, *112*, 083902.
(22) Kattoor, V.; Awasthi, K.; Jokar, E.; Diau, E. W.-G.; Ohta, N. Integral Method Analysis of Electoabsorption Spectra and Electrophotoluminescence Study of $(C_4H_9NH_3)_2PbI_4$ Organic-Inorganic Quantum Well. *J. Phys. Chem. C* **2018**, *122*, 26623−26634.
(23) Rana, S.; Awasthi, K.; Bhosale, S. S.; Diau, E. W.-G.; Ohta, N. Temperature-Dependent Electroabsorption and Electrophotoluminescence and Exciton Binding Energy in $MAPbBr_3$ Perovskite Quantum Dots. *J. Phys. Chem. C* **2019**, *123*, 19927−19937.
(24) Kattoor, V.; Awasthi, K.; Jokar, E.; Diau, E. W.-G.; Ohta, N. Enhanced Dissociation of Hot Excitons with an Applied Electric Field under Low-power Photoexcitation in Two-dimensional Perovskite Quantum Wells. *J. Phys. Chem. Lett.* **2019**, *10*, 4752−4757.
(25) Pollak, F. H.; Glembocki, O. J. Modulation Spectroscopy of Semiconductor Microstructures: An Overview. In *Spectroscopic Characterization Techniques for Semiconductor Technology III*; International Society for Optics and Photonics, 1988; Vol. *946*, pp 2−35.
(26) Aspnes, D. E. Modulation Spectroscopy/Electric Field Effects on the Dielectric Function of Semiconductors. In *Handbook on Semiconductors, Optical Properties of Solids*; North-Holland Publishing Co.: Amsterdam, 1980; Vol. *2*, pp 109−154.
(27) Aspnes, D. E. Direct Verification of the Third-Derivative Nature of Electroreflectance Spectra. *Phys. Rev. Lett.* **1972**, *28*, 168−171.
(28) Saba, M.; Cadelano, M.; Marongiu, D.; Chen, F.; Sarritzu, V.; Sestu, N.; Figus, C.; Aresti, M.; Piras, R.; Geddo Lehmann, A. G.; Cannas, C.; Musinu, A.; Quochi, F.; Murga, A.; Bongiovanni, G. Correlated Electron-Hole Plasma in Organometal Perovskites. *Nat. Commun.* **2014**, *5*, 5049.
(29) Even, J.; Pedesseau, L.; Katan, C. Analysis of Multivalley and Multibandgap Absorption and Enhancement of Free Carriers Related to Exciton Screening in Hybrid Perovskites. *J. Phys. Chem. C* **2014**, *118*, 11566−11572.
(30) Yamada, Y.; Nakamura, T.; Endo, M.; Wakayama, A.; Kanemitsu, Y. Photoelectronic Responses in Solution-Processed Perovskite $CH_3NH_3PbI_3$ Solar Cells Studied by Photoluminescence and Photoabsorption Spectroscopy. *IEEE J. Photovoltaics* **2015**, *5*, 401−405.
(31) Soufiani, A. M.; Huang, F.; Reece, P.; Sheng, R.; Ho-Baillie, A.; Green, M. A. Polaronic Exciton Binding Energy in Iodide and Bromide Organic-Inorganic Lead Halide Perovskites. *Appl. Phys. Lett.* **2015**, *107*, 231902.
(32) Yang, Y.; Yang, M.; Li, Z.; Crisp, R.; Zhu, K.; Beard, M. C. Comparison of Recombination Dynamics in $CH_3NH_3PbBr_3$ and $CH_3NH_3PbPbI_3$ Perovskite Films: Influence of Exciton Binding Energy. *J. Phys. Chem. Lett.* **2015**, *6*, 4688−4692.
(33) Yang, Y.; Ostrowski, D. P.; France, R. M.; Zhu, K.; van der Lagemaat, J.; Luther, J. M.; Beard, M. C. Observation of a Hot-Phonon Bottleneck in Lead-Iodide Perovskites. *Nat. Photonics* **2016**, *10*, 53−59.
(34) Sestu, N.; Cadelano, M.; Sarritzu, V.; Chen, F.; Marongiu, D.; Piras, R.; Mainas, M.; Quochi, F.; Saba, M.; Mura, A.; Bongiovanni, G. Absorption F-Sum Rule for the Exciton Binding Energy in Methylammonium Lead Halide Perovskites. *J. Phys. Chem. Lett.* **2015**, *6*, 4566−4572.
(35) Sun, S.; Salim, T.; Mathews, N.; Duchamp, M.; Boothroyd, C.; Xing, G.; Sum, T. C.; Lam, Y. M. The Origin of High Efficiency in Low-Temperature Solution-Processable Bilayer Organometal Halide Hybrid Solar Cells. *Energy Environ. Sci.* **2014**, *7*, 399−407.
(36) Savenije, T. J.; Ponseca, C. S.; Kunneman, L.; Abdellah, M.; Zheng, K.; Tian, Y.; Zhu, Q.; Canton, S. E.; Scheblykin, I. G.; Pullerits, T.; Yartsev, A.; Sundström, V. Thermally Activated Exciton Dissociation and Recombination Control the Carrier Dynamics in Organometal Halide Perovskite. *J. Phys. Chem. Lett.* **2014**, *5*, 2189−2194.
(37) Zhang, Q.; Ha, S. T.; Liu, X.; Sum, T. C.; Xiong, Q. Room-Temperature Near-Infrared High-Q Perovskite Whispering-Gallery Planar Nanolasers. *Nano Lett.* **2014**, *14*, 5995−6001.
(38) Tombe, S.; Adam, G.; Heilbrunner, H.; Apaydin, D. H.; Ulbricht, C.; Sariciftci, N. S.; Arendse, C. J.; Iwuoha, E.; Scharber, M.

https://dx.doi.org/10.1021/acsaem.0c01983
ACS Appl. Energy Mater. 2020, 3, 11830−11840

C. Optical and Electronic Properties of Mixed Halide (X = I, Cl, Br) Methylammonium Lead Perovskite Solar Cells. *J. Mater. Chem. C* **2017**, *5*, 1714−1723.
(39) Sun, X. G.; Shi, Z. F.; Li, Y.; Lei, L. Z.; Li, S.; Wu, D.; Xu, T. T.; Tian, Y. T.; Li, X. J. Effect of CH 3 NH 3 I Concentration on the Physical Properties of Solution-Processed Organometal Halide Perovskite $CH_3NH_3PbI_3$. *J. Alloys Compd.* **2017**, *706*, 274−279.
(40) D'Innocenzo, V.; Grancini, G.; Alcocer, M. J. P.; Kandada, A. R. S.; Stranks, S. D.; Lee, M. M.; Lanzani, G.; Snaith, H. J.; Petrozza, A. Excitons versus Free Charges in Organo-Lead Tri-Halide Perovskites. *Nat. Commun.* **2014**, *5*, 3586.
(41) Hirasawa, M.; Ishihara, T.; Goto, T.; Uchida, K.; Miura, N. Magnetoabsorption of the Lowest Exciton in Perovskite-Type Compound $(CH_3NH_3)PbI_3$. *Phys. B* **1994**, *201*, 427−430.
(42) Tanaka, K.; Takahashi, T.; Ban, T.; Kondo, T.; Uchida, K.; Miura, N. Comparative Study on the Excitons in Lead-Halide-Based Perovskite-Type Crystals $CH_3NH_3PbBr_3$ $CH_3NH_3PbI_3$. *Solid State Commun.* **2003**, *127*, 619−623.
(43) Miyata, A.; Mitioglu, A.; Plochocka, P.; Portugall, O.; Wang, J. T. W.; Stranks, S. D.; Snaith, H. J.; Nicholas, R. J. Direct Measurement of the Exciton Binding Energy and Effective Masses for Charge Carriers in Organic-Inorganic Tri-Halide Perovskites. *Nat. Phys.* **2015**, *11*, 582−587.
(44) Galkowski, K.; Mitioglu, A.; Miyata, A.; Plochocka, P.; Portugall, O.; Eperon, G. E.; Wang, J. T.-W.; Stergiopoulos, T.; Stranks, S. D.; Snaith, H. J.; Nicholas, R. J. Determination of the Exciton Binding Energy and Effective Masses for Methylammonium and Formamidinium Lead Tri-halide Perovskite Semiconductors. *Energy Environ. Sci.* **2016**, *9*, 962−970.
(45) Yang, Z.; Surrente, A.; Galkowski, K.; Bruyant, N.; Maude, D. K.; Haghighirad, A. A.; Snaith, H. J.; Plochocka, P.; Nicholas, R. J. Unraveling the Exciton Binding Energy and the Dielectric Constant in Single-Crystal Methylammonium Lead Triiodide Perovskite. *J. Phys. Chem. Lett.* **2017**, *8*, 1851−1855.
(46) Lin, Q.; Armin, A.; Nagiri, R. C. R.; Burn, P. L.; Meredith, P. Electro-optics of Perovskite Solar Cells. *Nat. Photonics* **2015**, *9*, 106−112.
(47) Grancini, G.; Kandada, A. R. S.; Frost, J. M.; Barker, A. J.; Bastiani, M. D.; Gandini, M.; Marras, S.; Lanzani, G.; Walsh, A.; Petrozza, A. Role of Microstructure in the Electron-Hole Interacation of Hybrid Lead Halide Perovskites. *Nat. Photonics* **2015**, *9*, 695−702.
(48) Umeuchi, S.; Nishimura, Y.; Yamazaki, I.; Murakami, H.; Yamashita, M.; Ohta, N. Electric Field Effects on Absorption and Fluorescence Spectra of Pyrene Doped in a PMMA Polymer Film. *Thin Solid Films* **1997**, *311*, 239−245.
(49) Varshni, Y. P. Temperature Dependence of the Energy Gap in Semiconductors. *Physica* **1967**, *34*, 149−154.
(50) Awasthi, K.; Kala, K.; Rana, S.; Diau, E. W.-G.; Ohta, N. Switching between Spectral Broadening and Narrowing of the Exciton Absorption Band of a $CH_3NH_3PbI_3$ Film on Altering the Polarity of an Applied Electric Field. *Appl. Phys. Lett.* **2020**, *116*, 251101.
(51) Liptay, W. Dipole Moments and Polarizabilities of Molecules in Excited Electronic States. In *Excited States*; Lim, E. C., Ed.; Academic Press: New York, 1974; Vol. *1*, pp 129−229.
(52) Bublitz, G. U.; Boxer, S. G. Stark Spectroscopy: Applications in Chemistry, Biology, and Materials Science. *Annu. Rev. Phys. Chem.* **1997**, *48*, 213−242.
(53) Locknar, S. A.; Peteanu, L. A. Investigation of the Relationship between Dipolar Properties and Cis-Trans Configuration in Retinal Polyenes: A Comparative Study Using Stark Spectroscopy and Semiempirical Calculations. *J. Phys. Chem. B* **1998**, *102*, 4240−4246.
(54) Jalviste, E.; Ohta, N. Theoretical Foundation of Electro-absorption Spectroscopy: Self-Contained Derivation of the Basic Equations with the Direction Cosine Method and the Euler Angle Method. *J. Photochem. Photobiol., C* **2007**, *8*, 30−46.
(55) Awasthi, K.; T. Iimori, T.; Ohta, N. Integral Method Analysis of Electroabsorption Spectra and Its Application to Quantum Dots of PbSe. *J. Phys. Chem. C* **2014**, *118*, 18170−18176.
(56) Chen, J.; Shi, T.; Li, X.; Zhou, B.; Cao, H.; Wang, Y. Origin of the High Performance of Perovskite Solar Cells with Large Grains. *Appl. Phys. Lett.* **2016**, *108*, 053302.
(57) Kim, H.; Ohkita, H.; Benten, H.; Ito, S. Photovoltaic Performance of Perovskite Solar Cells with Different Grain Sizes. *Adv. Mater.* **2016**, *28*, 917−922.
(58) Elliott, R. J. Intensity of Optical Absorption by Excitons. *Phys. Rev.* **1957**, *108*, 1384−1389.
(59) Rudin, S.; Reinecke, T. L.; Segal, B. Temperature-Dependent Exciton Linewidths in Semiconductors. *Phys. Rev. B* **1990**, *42*, 11218−11231.
(60) Phuong, L. Q.; Yamada, Y.; Nagai, M.; Maruyama, N.; Wakamiya, A.; Kanemitsu, Y. Free Carriers versus Excitons in $CH_3NH_3PbI_3$ Perovskite Thin Films at Low Temperatures: Charge Transfer from the Orthorhombic Phase to the Tetragonal Phase. *J. Phys. Chem. Lett.* **2016**, *7*, 2316−2321.
(61) Phuong, L. Q.; Nakaike, Y.; Wakamiya, A.; Kanemitsu, Y. Free Excitons and Exciton-Phonon Coupling in $CH_3NH_3PbI_3$ Single Crystals Revealed by Photocurrent and Photoluminescence Measurements at Low Temperatures. *J. Phys. Chem. Lett.* **2016**, *7*, 4905−4910.
(62) Zhu, X.-Y.; Podzorov, Y. Charge Carriers in Hybrid Organic-Inorganic Halide Perovskites Might Be Protected as Large Polarons. *J. Phys. Chem. Lett.* **2015**, *6*, 4758−4761.
(63) Wright, A. D.; Verdi, C.; Milot, R. L.; Eperon, G. E.; Pérez-Osorio, M. A.; Snaith, H. J.; Giustino, F.; Johnston, M. B.; Herz, L. M. Electron-Phonon Coupling in Hybrid Lead Halide Perovskites. *Nat. Commun.* **2016**, *7*, No. 11755.
(64) Kandada, A. R. S.; D'Innocenzo, V.; Lanzani, G.; Petrozza, A. A. Photophysics of Hybrid Perovskites. In *Unconventional Thin Film Photovoltaics*; Como, E. D.; Angelis, F. D.; Snaith, H.; Walker, A., Eds.; RSC Energy and Environment Series; Royal Society of Chemistry, 2016; Vol. *16*, Chapter 4, pp 107−140.
(65) Soufiani, A. M.; Yang, Z.; Young, T.; Miyata, A.; Surrente, A.; Pascoe, A.; Galkowski, K.; Abdi-Jalebi, M.; Brenes, R.; Urban, J.; Zhang, N.; Bulovic, V.; Portugall, O.; Cheng, Y.-B.; Nocholas, R. J.; Ho-Baillie, A.; Green, M. A.; Plochocka, P.; Stranks, S. D. Impact of Microstructure on the Electron-Hole Interaction in Lead Halide Perovskites. *Energy Environ. Sci.* **2017**, *10*, 1358−1366.
(66) Poglitsch, A.; Weber, D. Dynamic Disorder in Methylammoniumtrihalogenoplumbates (II) Obsrved by Millimeter-Wave Spectroscopy. *J. Chem. Phys.* **1987**, *87*, 6373−6378.

https://dx.doi.org/10.1021/acsaem.0c01983
ACS Appl. Energy Mater. 2020, 3, 11830−11840